Talanta 116 (2013) 223–230

Contents lists available at ScienceDirect

Talanta

journal homepage: www.elsevier.com/locate/talanta

A novel nonenzymatic sensor based on CuO nanoneedle/graphene/carbon nanofiber modified electrode for probing glucose in saliva

Daixin Ye, Guohai Liang, Huixiang Li, Juan Luo, Song Zhang, Hui Chen, Jilie Kong *

Department of Chemistry and Institutes of Biomedical Sciences, Fudan University, Shanghai 200433, PR China

ARTICLE INFO

Article history:
Received 16 January 2013
Received in revised form
28 March 2013
Accepted 4 April 2013
Available online 30 April 2013

Keywords:
Glucose
Graphene
Carbon fiber
CuO nanoneedle

ABSTRACT

Here, we report on a novel nonenzymatic amperometric glucose sensor based on CuO nanoneedle/graphene/carbon nanofiber modified electrode. The results of the scanning electron microscopy indicate that electronic network was formed through their direct binding with the graphene/carbon nanofiber, which leads to larger active surface areas and faster electron transfer for the glucose sensor. High electrocatalytic activity toward the oxidation of glucose was observed with a rapid response (<2 s), a low detection limit (0.1 μM), a wide and useful linear range (1–5.3 mM) as well as good stability and repeatability. Moreover, the common interfering species, such as ascorbic acid, uric acid, dopamine and so forth did not cause obvious interference. The sensor can also be used for quantification of glucose concentration in real saliva samples. Therefore, this work has demonstrated a simple and effective sensing platform for nonenzymatic detection of glucose.

1. Introduction

Diabetes mellitus is a chronic but treatable disease affecting about 200 million people around the world. For these patients, regular measurements of blood glucose levels are required to confirm whether the treatments are working effectively [1]. As a result, there is an ever-growing demand to create high sensitivity, high reliability, rapid, recyclable low cost and non-invasive glucose sensors. There are now many approaches to measure glucose concentration, such as the optical techniques including infrared spectroscopy, Raman spectroscopy, and photo acoustic spectroscopy [2,3], surface plasmon resonance biosensor [4], capacitive detection [5], electrochemiluminescene, colorimetry [6], the electrochemical method [7–9], and so forth. Among these techniques, the electrochemical approach has attracted significant attention and has become a promising method for its simplicity, high reliability, sensitivity, selectivity, low detection limit, low cost, compatibility for miniaturization, and ease of use. Electrochemical sensors for glucose determination are basically classified into two major types which are enzymatic and nonenzymatic modified sensors. However, the enzymatic glucose sensors have a great drawback that is their lack of stability originating from the intrinsic nature of the enzymes, which is hard to overcome. The activity of enzymes can also be easily affected by temperature, solution pH, humidity, and toxic chemicals. Although glucose oxidase (GOD) is quite stable compared with other enzymes, GOD-based glucose sensors have always come across thermal and chemical deformation. Therefore, nonenzymatic amperometric biosensors drew more interest recently, especially for the nonenzymatic glucose sensors based on metal or metal oxide. While the sensitivity and the signal-to-noise ratio (SNR) of these sensors still need to be improved.

Up to now, most of the reported glucose sensors have been using the blood sample. For a health man, the blood glucose range is 3.6–7.5 mM (65–135 mg/dL), while for diabetic patients, it is 1.1–20.8 mM (20–350 mg/dL). Noninvasive route for continuous glucose monitoring is highly expected to eliminate pain and discomfort associated with implantable devices. So, noninvasive glucose sensing is the ultimate goal for routine glucose monitoring. Saliva is a relatively good candidate for noninvasive determination of glucose; however, the concentration of glucose in saliva is very low, usually from 30 to 80 μM, obviously lower than the detection limit of normal glucose seniors for blood, which thus inspired us to exploit glucose sensors with lower detection limit.

Nanostructured materials are well known to be much more efficient and selective than traditional bulk materials for their high surface areas and high surface energy. For example, many carbon-based nanostructure materials have been shown to be ideal for biosensing applications since they are conductive, biocompatible, easily functionalized, and possess very large surface areas. On the other hand, as a p-type semiconductor with a narrow band gap of 1.2 eV, CuO has been widely studied because of its numerous applications in catalysis, semiconductors, gas sensors, biosensors, and field transistors [10,11]. E. Reitz et al. [12] have reported CuO

* Corresponding author. Tel.: +86 21 6564 2138; fax: +86 21 6564 1740.
E-mail address: jlkong@fudan.edu.cn (J. Kong).

0039-9140/$ - see front matter © 2013 Published by Elsevier B.V.
http://dx.doi.org/10.1016/j.talanta.2013.04.008

nanospheres based nonenzymatic glucose sensor with a linear range of 0.05–2.25 mM. Wang et al. [13] have prepared a nonenzymatic glucose sensor using a novel Cu–CuO nanowire composite. The reported sensors displayed low detection limits (~0.05 mM); however, they were not low enough for the demand of glucose determination in saliva.

Based on the above information, here, we constructed a novel nonenzyme glucose sensor based on CuO nanoneedle/graphene/carbon nanofiber modified glassy carbon electrode (CuO/rGO/CNF/GCE) to resolve the problems appearing in the analysis of glucose in saliva. To the best of our knowledge, the simultaneous preparation of nanoneedle CuO and flower like CuO can not only greatly enlarge the specific surface area of the electrode but also have high catalytic effect on the oxidation of glucose. 1D carbon nanofibers (CNFs) and 2D reduced graphene oxide (rGO) have been extensively studied in electrochemical sensors [14,15]. Combination of them to form a new composite may produce a synergistic effect. The CNFs in the rGO/CNFs film not only efficiently increase the basal spacing but also bridge the defects for electron transfer between rGO nanosheets [16]. Thus, the unique rGO/CNFs film, displays even better electrochemical performance and higher electronic conductivity than the single-component rGO film [16]. And also, the rGO/CNFs film would be a perfect substrate to deposit CuO for electrochemistry sensors applications in view of its admirable electronic conductivity. As expected, the as-prepared CuO/rGO/CNF/GCE exhibits a wide liner response range with increased sensitivity and improved SNR. Moreover, the glucose level in saliva was detected with ideal reproducibility. Therefore, this work provides an excellent platform for non-invasive determination of glucose for diabetic patients.

2. Experimental

2.1. Apparatus and chemicals

Graphite powder and hydrazine solution (35 wt% in water) were purchased from Sigma-Aldrich. Carbon nanofiber was purchased from Japanese Showa Co. Ltd. All experiments were performed in 0.1 M NaOH solution and double distilled water was used throughout. All electrochemical experiments were carried out at room temperature 25 ± 0.1°C.

Electrochemical experiments including cyclic voltammetry (CV) and amperometry were carried out on CHI 660 A electrochemical workstation (Chenhua, Shanghai, China). Electrochemical impedance spectroscopy (EIS) was carried out on Autolab PGSTST 30 analyzer (Metrohm Autolab B.V., Switzerland). A conventional three-electrode electrochemical system was used for all electrochemical experiments, which consisted of a working electrode, a Pt foil auxiliary electrode and a saturated calomel electrode. A GCE was used as the basal working electrode. Transmission electron microscopy (TEM) and scanning electron microscopy (SEM) images were taken with a JEOL2011microscope (Japan) operated at 200 kV and a Philips XL30 electron microscope (The Netherlands) operated at 10 kV, respectively. X-ray photoelectron spectra (XPS) were carried out on a RBD upgraded PHI-5000C ESCA system (PerkinElmer). The EDS spectra were measured during the SEM measurements. Raman spectra were recorded on a LabRam-1B microscopic confocal Raman spectrometer (Jobin Yvon, France).

2.2. Preparation of modified electrodes

Graphene oxide was synthesized from graphite powder via a modified Hummers and Offeman method [17]. Reduction of graphene oxide was performed using hydrazine as described by Stankovich et al. [18]. Prior to use, the GCE was polished with 0.3 and 0.05 μm α-Al_2O_3 powder until a mirror-shiny surface was obtained, then ultrasonicated in ethanol and double distilled water for 10 min. Finally, it was dried under a stream of high purity nitrogen for further use. 1 mg rGO was homogeneously dispersed in 1 mL N-Methyl pyrrolidone (NMP) and 2 mg carbon nanofiber (CNF) was dispersed in 1 mL NMP at room temperature with the aid of ultrasonic agitation. Then the above suspensions were mixed with the same volume and ultrasonicated to obtain homogeneously dispersed rGO/CNF composite. 5 μL of the resulting mixture was dropped onto the cleaned GCE surface to prepare rGO/CNF/GCE and the modified electrode was allowed to dry under an infrared lamp. Cu was electrodeposited on the rGO/CNF/GCE by maintaining potential at −0.40 V for 210 s in 0.1 M KCl solution containing 0.01 M $CuCl_2$ and the obtained electrode was named as Cu/rGO/CNF/GCE. After washing with water and drying with a flow of N_2, the Cu/rGO/CNF/GCE was immersed in 0.1 M NaOH and repeatedly scanned with CV under the potential range from −0.50 to +0.30 V at 100 mV s^{-1} until a stable condition is reached. During the repetitive cyclic potential scanning in the supporting solution of 0.1 M NaOH, CuO nanoneedles were formed on the rGO/CNF. The possible mechanism of the electrodeposition can be shown below [19]:

$$Cu + OH^- \rightarrow CuOH + e^- \quad (1)$$

$$2CuOH + 2OH \rightarrow Cu_2O + H_2O + 2e^- \quad (2)$$

$$CuOH + OH \rightarrow CuO + H_2O \quad (3)$$

$$Cu_2O + 2OH^- \rightarrow CuO + H_2O^- + e^- \quad (4)$$

Finally, the electrode was rinsed with water and dried with a flow of N_2. The as-prepared modified electrode was named as CuO/rGO/CNF/GCE. The obtained CuO/rGO/CNF/GCE was preserved in a refrigerator at 4 ℃ after being washed with double distilled water. The specific process is shown in scheme 1. CuO nanoneedles were electrochemically deposited onto the rGO/CNF and the resulting nanocomposite generates electrochemical signals in the presence of glucose.

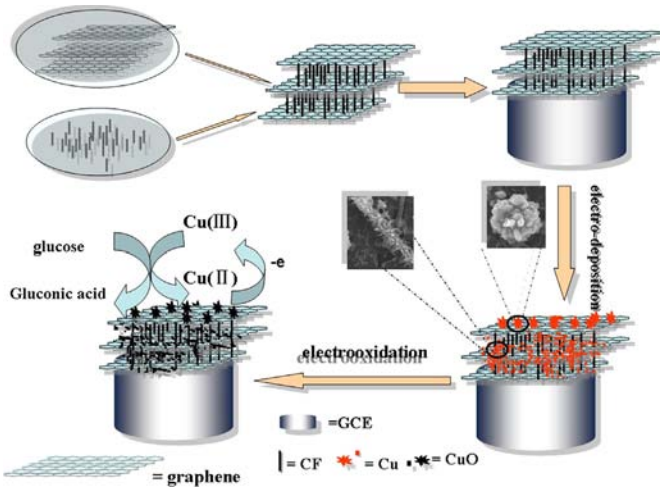

Scheme 1. A schematic diagram (not to scale) of the fabrication and application of CuO/rGO/CNF/GCE glucose sensor. CuO nanoparticles are electrochemically deposited onto the rGO/CNF and the resulting nanocomposite generates electrochemical signals in the presence of glucose.

2.3. Sample preparation for SEM, EIS, Raman spectroscopy, XPS and TEM study characterization

A glassy carbon plate (GCP) was polished with 0.05 μM alumina powders, then sonicated in 1:1 HNO_3, ethanol and double distilled water and dried at room temperature. The rGO/CNF/GCP was prepared by casting rGO/CNF suspensions onto the surface of GCP. Cu was electrodeposited on the rGO/CNF modified GCP by maintaining potential at −0.40 V for 210 s in 0.1 M KCl solution containing 0.01 M $CuCl_2$ and the obtained GCP was named as Cu/rGO/CNF/GCP. After washing with water and drying with a flow of N_2, the Cu/rGO/CNF/GCP was immersed in 0.1 M NaOH and repeatedly scanned with cyclic voltammetry under the potential range from –0.50 to +0.30 V at 100 mV s^{-1} until a stable condition is reached. The obtained GCP was named as CuO/rGO/CNF/GCP. The prepared rGO/CNF/GCP and CuO/rGO/CNF/GCP were used for SEM, EIS, Raman spectroscopy and XPS studies. For TEM study, a certain amount of rGO was dispersed in ethanol absolute with the aid of ultrasonic agitation, and then a drop of the suspensions was dropped on carbon film and allowed to dry under an infrared lamp.

2.4. Preparation of saliva sample

Saliva samples were collected from healthy volunteers after rinsing their mouths with water. The obtained saliva samples were centrifuged at 2000 r/min for 30 min and the supernatants were collected and stored at −20 °C until analysis

3. Results and discussion

3.1. Characterization of the modified electrodes

The morphology of rGO was characterized by TEM and SEM. As shown in Fig. 1A, the rGO presents nearly transparent flake-like shape. The SEM image of rGO is displayed in Fig. 1B. The rGO sheets were crumpled and wrinkled on the surface of the glassy carbon substrate, which provided an ideal matrix for the distribution of CuO. Fig. 1C shows the SEM image of rGO and CNF composite, from which we can see that rGO and CNF were mixed uniformly, and CNF was well distributed among the layers of rGO. Fig. 1D and E were the SEM images of CuO/rGO/CNF composite

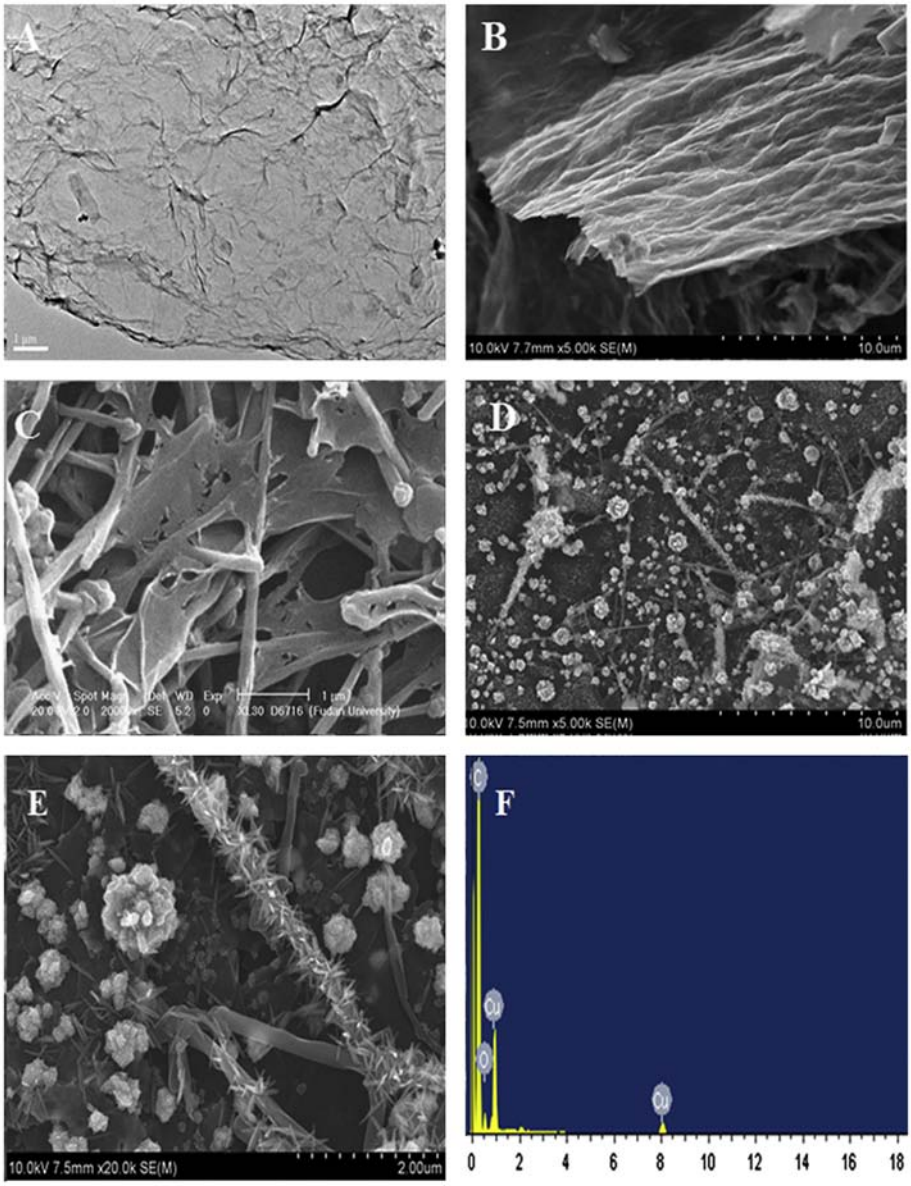

Fig. 1. TEM image of rGO (A), SEM image of rGO (B), rGO/CNF (C), CuO/rGO/CNF (D), the magnified image CuO/rGO/CNF (E) and EDS of CuO/rGO/CNF (F).

with low and high magnification, respectively. A large number of flowers like aggregates equally distributed in glassy carbon substrate can be observed from Fig. 1D. For the magnified image, one can see that the aggregates are mainly composed of numerous closely packed nanoneedles extending from the inner part of the aggregates. And also, some other nanoneedles were compactly distributed on the CNF and rGO. Thus, the presences of nanoneedle CuO greatly enlarge the specific surface area of the electrode. The energy dispersive X-ray (EDX) spectra of the CuO in Fig. 1F shows that only Cu, C and O are the elemental components, implying no other impurity in the prepared samples.

Structural analyses of the rGO, rGO/CNF, CuO/rGO/CNF nanostructures were carried out by Raman spectroscopy in the range of 200–2000 cm^{-1} measured at room temperature, and the results are shown in Fig. 2. The CuO crystal belongs to the C_{2h}^6 space group with two molecules per primitive cell. Three Raman-active modes (Ag+2Bg) were observed. We can assign the peak at 297 cm^{-1} to the Ag mode and the peaks at 346 and 631 cm^{-1} to the Bg modes, which are consistent with the previous reports [20]. The peaks at 1594 and 1332 cm^{-1} correspond to the well-documented G and D bands, respectively, which are characteristic peaks of carbon material. The G band represents the first-order scattering of the E_{2g} vibrational mode while the D band has been attributed to the reduction in size of the in-plane C sp^2 atoms.

The purity and the composition of the CuO nanoneedles were further investigated by X-ray photoelectron spectroscopy (Fig. 3). The full scan spectrum demonstrates the presence of Cu and O (Fig. 3A).The peaks at about 936.6 and 956.2 eV are attributed to Cu $2p_{3/2}$ and $2p_{1/2}$ (Fig. 3B), respectively. The main peak at 936.6 eV is accompanied by the strong shake up satellite peak present at 945.4 eV. This feature is characteristic of the Cu (II) state. The existence of strong satellite features for Cu 2p rules out the possibility of the presence of the Cu_2O phase in the prepared nanocomposite [21].

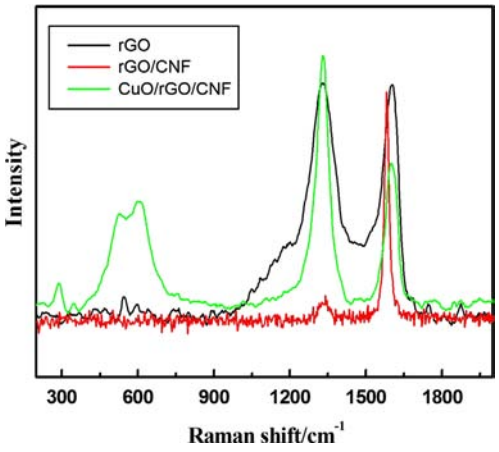

Fig. 2. Raman spectra of rGO, rGO/CNF, CuO/rGO/CNF.

3.2. Electrochemical catalytic oxidation of glucose on the CuO/rGO/CNF/GCE

The electrocatalytic properties of the CuO/rGO/CNF/GCE, CuO/rGO/GCE, CuO/CNF/GCE, CuO/GCE, and bare GCE were investigated by CV in 0.1 M NaOH solution with 3.0 mM glucose, as shown in Fig. 4A. There is no obvious oxidation peak which could be observed on the bare GCE; however, after modification of CuO, oxidation current of glucose appeared. Interestingly, after further modification of CNF, or rGO, the oxidation current of glucose becomes markedly larger, indicating that CNF, or rGO accelerated the electron transfer rate. Compared with CuO/rGO/GCE, CuO/CNF/GCE, CuO/GCE, and bare GCE, CuO/rGO/CNF/GCE displays the highest oxidation peak current. The key factors for consideration of the excellent electrochemical performance of the CuO/rGO/CNF/GCE are based on the advantages that arise from its large surface area, high porosity, and highly conductive matrix. 1D CNF and 2D rGO can easily form high porosity and electrical network structure; meanwhile, CNFs in the rGO/CNF film not only efficiently increase the basal spacing but also bridge the defects for electron transfer between rGO nanosheets. Thus, the conductivity was highly increased. Part B in Fig. 4 shows the CVs of the CuO/rGO/CNF/GCE in the presence (curve b) and absence (curve a) of glucose (3 mM) in 0.1 M NaOH solution. In the absence of glucose, a single somewhat broad reduction peak with the potential of about 0.58 V was observed, which corresponds to the Cu (II)/Cu (III) redox couple similar to the previous report [22]. Upon addition of glucose (3 mM), an obvious oxidation peak corresponding to the irreversible glucose oxidation was observed.

The oxidation of glucose started at approximately +0.2 V, with a peak at about +0.48 V. As shown in Fig. 4B (curve a), no similar electrochemical response was observed in the same potential range (corresponding to glucose oxidation) in 0.1 M NaOH without glucose. The possible mechanism of electrocatalytic oxidation of glucose in alkaline electrolyte on the CuO modified electrode is generally considered to undergo the following steps.

The first step is that CuO is electrochemically oxidized to strong oxidizing agent Cu (III) species such as CuOOH, and then glucose is catalytically oxidized by the Cu (III) species and produce hydrolyzate gluconic acid. At the same time, Cu (III) species change into

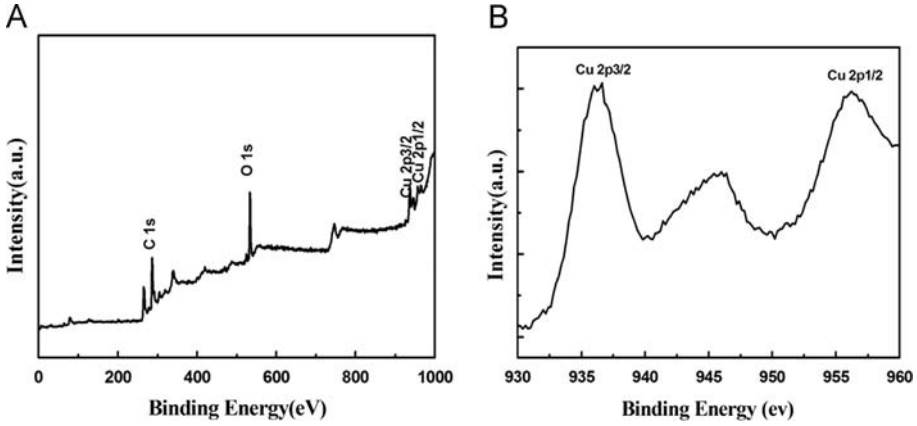

Fig. 3. XPS survey spectra (A) and Cu 2p XPS spectra of CuO (B).

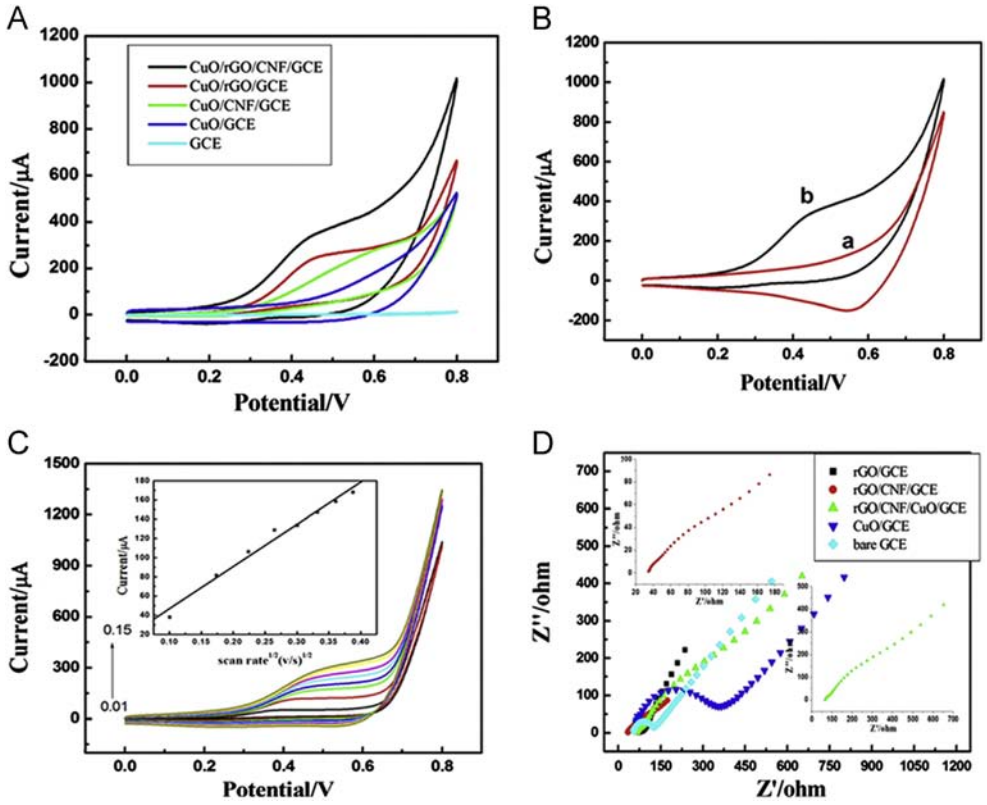

Fig. 4. CVs of CuO/rGO/CNF/GCE, CuO/rGO/GCE, CuO/CNF/GCE, CuO/GCE, bare GCE 0.1 M NaOH with 3 mM glucose at 100 mV s^{-1} (A); CVs of CuO/rGO/CNF/GCE in the absence (a) or presence (b) of 3 mM glucose, respectively (B); CVs of CuO/rGO/CNF/GCE 0.1 M NaOH containing 3 mM glucose at different scan rates from 10 to 150 mV s^{-1}. Inset shows the oxidation peak current vs. scan $rate^{1/2}$ (C) and Nyquist plots at GCE, rGO/CNF/GCE, rGO/GCE and CuO/rGO/CNF/GCE in 0.1 M KCl solution containing 5 mM $[Fe(CN)_6]^{3-/4-}$.

Cu (II). The specific equations are shown below:

$$CuO + OH^- \rightarrow CuOOH + e^- \quad (5)$$

$$Cu(III) + glucose \rightarrow Gluconolactone + Cu(II) \quad (6)$$

$$Gluconolactone \rightarrow Gluconic\ acid(hydrolysis) \quad (7)$$

The effects of different scan rates on the oxidation of glucose at the CuO/rGO/CNF/GCE are displayed in Fig. 4C. The peak current for the oxidation of glucose is proportional to the square root of the scan rate, indicating that the electrocatalytic reaction is diffusion controlled. Furthermore, the impedance measurements of the different electrodes in 0.1 M KCl solution containing 5 mM $[Fe(CN)_6]^{3-/4-}$ were also investigated, and the Nyquist plots for all electrodes are shown in Fig. 4D. As expected, after modification of rGO on the bare GCE, the plots exhibited much smaller semicircle in the high frequency region and steeper straight line in the low frequency region. The results indicate that the doping of rGO can decrease the electron transfer resistance and improve the heterogeneous electron transfer process. However, compared to a semicircle and a linear region of the bare GCE, CuO/GCE and rGO/GCE, CuO/rGO/CNF/GCE and rGO/CNF/GCE show approximate two semicircles and a linear region, which are quite similar to the impedance behavior of porous electrodes [23]. The change of currents of different electrodes in 0.1 M NaOH solutions at 0.6 V is also investigated. As shown in Fig. 5, the stable currents are about −1.03, −0.59, and −0.13 μA for CuO/GCE, CuO/rGO/GCE, and CuO/rGO/CNF/GCE, respectively. The small background currents of CuO/rGO/CNF/GCE make it appropriate as the substrate materials of biosensors, especially when the concentration of the detected object is low. Moreover, it can stabilize rapidly within about 10 s, which is less than the other two electrodes.

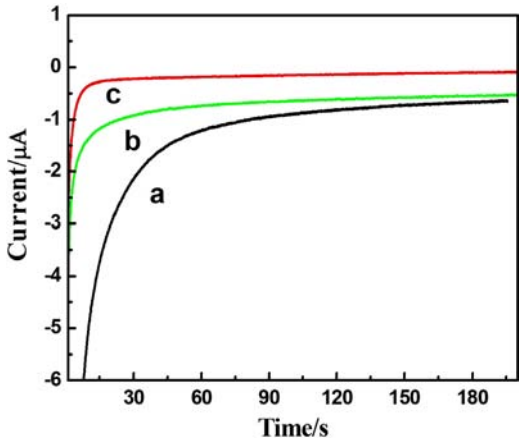

Fig. 5. Change of currents on different electrodes: CuO/GCE (a), CuO/rGO/GCE (b), and CuO/rGO/CNF/GCE (c), at 0.6 V in 0.1 M NaOH solution without stirring.

3.3. Optimization of the sensing conditions

The influence of the electrodeposition time on the electrocatalytic activity of the nanocomposite electrode toward glucose oxidation was investigated. As shown in Fig. 6A, the peak current response increased with the increment of Cu electrodeposition time and achieved a maximum value at 210 s. With the increasing of Cu electrodeposition time from 210 to 260 s, the current decreased gradually. Therefore, 210 s was used as an optimized Cu electrodeposition time in subsequent experiments.

Since the catalytic reaction of glucose oxidation requires the presence of OH^- ions, and therefore the effect of NaOH

concentration on the response of glucose was investigated as shown in Fig. 6B. The current response of the CuO/rGO/CNF/GCE increased from 0.01 to 0.1 M of NaOH. However, the current response decreased and the background current increased in higher NaOH concentrations. Thus, 0.1 M of NaOH was chosen as the optimal supporting electrolyte.

In order to obtain optimal amperometric response to glucose, the effect of different applied potentials on the response current of

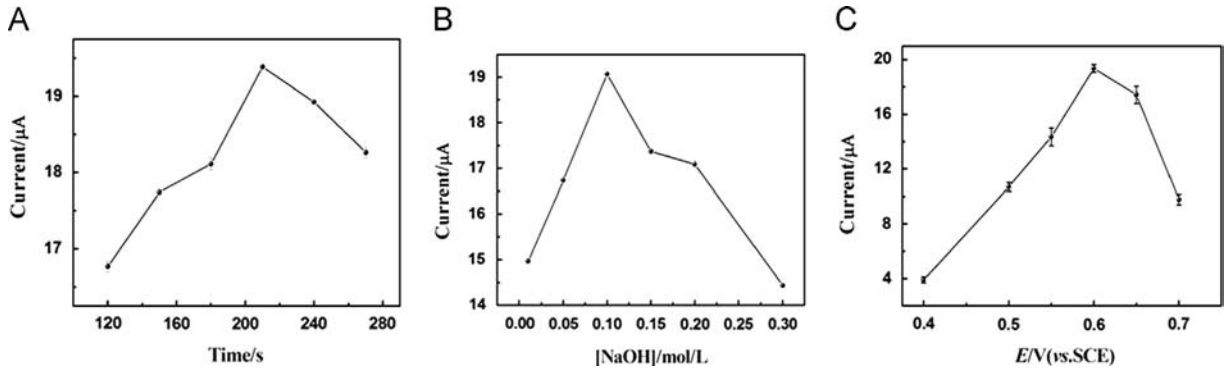

Fig. 6. Effects of deposition time (A), NaOH concentration (B) and applied potential (C) on the amperometric response of the CuO/rGO/CNF/GCE toward 0.1 mM glucose. Error bars represent the standard deviation of 3 independent experiments.

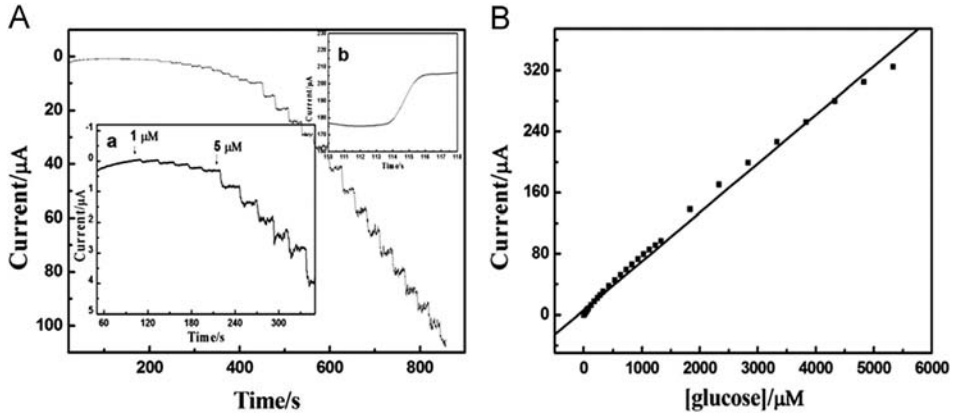

Fig. 7. Current–time responses of CuO/rGO/CNF/GCE on successive addition of different concentrations of glucose to 0.1 M NaOH (A); insets in Fig. 7A: the current response toward low concentrations of glucose (a); the response time of CuO/rGO/CNF/GCE to achieve steady-state current (b); and calibration curve of concentration vs. peak current of glucose (B).

Table 1
Comparison of analytical performance of our proposed CuO/rGO/CNF/GCE sensor with other published glucose sensors.

Modified electrode	Linear working range (μM)	Response speed (s)	Detection limit (μM)	Reproducibility (%)
PdNPs/FCNTs/GCE [24]	0–46000	–	–	4.31 ($n=10$)
BDDNF electrode [25]	0–7000	<20	0.2	–
rGO/GOD/PFIL/GCE [26]	2000–14000	–	–	3.2 ($n=8$)
GOD/rGO/chitosan/GCE [27]	80–12000	–	20	5.3 ($n=6$)
Cu-rGO sheets		<2	0.5	
Electrode [28]	Up to 4500			4.8 ($n=5$)
PdNPs/rGO/Nafion [29]	10–5000	9	1	3.4 ($n=10$)
GOD-PEDOT/PtNP/MGPNs [30]	10–50000	5	0.3	–
NiCFP [31]	2–2500	5	1	3.9 ($n=6$)
NTAEs [32]	2–14000	–	1	–
rGO/AuNPs/GOD/chitosan/Au electrode [33]	2500–7500	–	180	4.7 ($n=6$)
Nafion/GOD/Ag-Pdop@CNT/GCE [34]	50–1100	<5	17	1.5 ($n=9$)
CuO flowers [35]	4–8000	10	4	–
CuO/copper oxalate/ copper strip [36]	**2–15000**	–	**0.05**	–
Ni-powder/CCE [37]	**0.5–5000**	$<$ **1**	**0.1**	**3** (***n*****=6**)
This work	1–5300	<2	0.1	2.2 ($n=10$)

PdNPs/FCNTs/GCE: palladium nanoparticles functional carbon nanotubes modified GCE; BDDNF electrode:boron-doped diamond nanorod forest electrode; PdNPs/rGO/Nafion: palladium nanoparticles functioned rGO modified electrode; rGO/GOD/PFIL/GCE: with glucose oxidase (GOD) as an enzyme model, polyvinylpyrrolidone-protected rGO/polyethylenimine-functionalized ionic liquid/GOD; Cu/rGO sheets electrode: electrodepositing metallic Cu nanoparticles on rGO sheets; GOD-PEDOT/PtNP/MGPNs: multilayered rGO petal nanosheets (MGPNs), Pt nanoparticles, and a biorecognition element GOD modified electrode; GOD/rGO/chitosan/GCE: GOD/rGO/chitosan nanocomposite modified electrode; NiCFP: renewable Ni nanoparticle-loaded carbon nanofiber paste electrode; rGO/AuNPs/GOD/chitosan/Au electrode: immobilization of glucose oxidase in thin films of chitosan containing nanocomposites of rGO and gold nanoparticles at a gold electrode; NTAEs: highly ordered platinum-nanotubule array electrode; and Ni-powder/CCE: Ni-powder modified carbon ceramic electrodes.

the sensor was also tested. As shown in Fig. 6C, the response current increased sharply along with the increase of applied potential until the potential reached +0.6 V. Therefore, +0.6 V was selected for the amperometric detection of glucose.

3.4. Electrochemical sensing of glucose

The amperometric responses at the CuO/rGO/CNF/GCE at a working potential of 0.6 V (vs. SCE) in 0.1 M NaOH solution for each successive addition of various concentrations of glucose are presented in Fig. 7. Upon each addition of glucose, electrochemical responses were recorded while the solution was stirred constantly. As shown in Fig. 7A, it is clear that the electrochemical response to glucose at the CuO/rGO/CNF/GCE is very fast in reaching a dynamic equilibrium upon each addition of the sample solution, generating a steady-state current signal within a short time (less than 3 s). Fig. 7B shows the calibration curve of glucose at the CuO/rGO/CNF/GCE. The proposed electrode gave a linear response to glucose in the range from 1 μM to 5.3 mM with a correlation coefficient of 0.997. The corresponding regression equation is I (μA)=6.298 +0.06389C (μM). The sensor has a high sensitivity of 912.7 μA mM^{-1} cm^{-2} and a low detection limit of 0.1 μM (S/N=3) for glucose sensing. For comparison, the performances of the CuO/rGO/CNF/GCE and other glucose sensors reported in literatures have been listed in Table 1. From Table 1, it can be concluded that the developed modified sensor has a higher sensitivity, a lower detection limit, and a quite wider linear range than those reported previously. The high sensitivity implies that the sensor has a high electrocatalytic activity toward the glucose oxidation due to the high catalytic activity of the CuO nanostructures and the electronic network formed through their direct binding with the rGO/CNF. Moreover, the well-distributed CuO nanoneedles on the rGO/CNF surface (Fig. 1) result in the catalyst being easily accessed by substrates, and hence, the S/N ratio can be greatly improved, and the catalytic efficiency can be significantly enhanced. Furthermore, the broad linear sensing range of the sensor not only enables sensing within the physiological range for blood glucose of healthy and diabetic patients, it enables glucose sensing in saliva, tears, and urine as well. These are the advantages of the developed sensor compared with those reported previously.

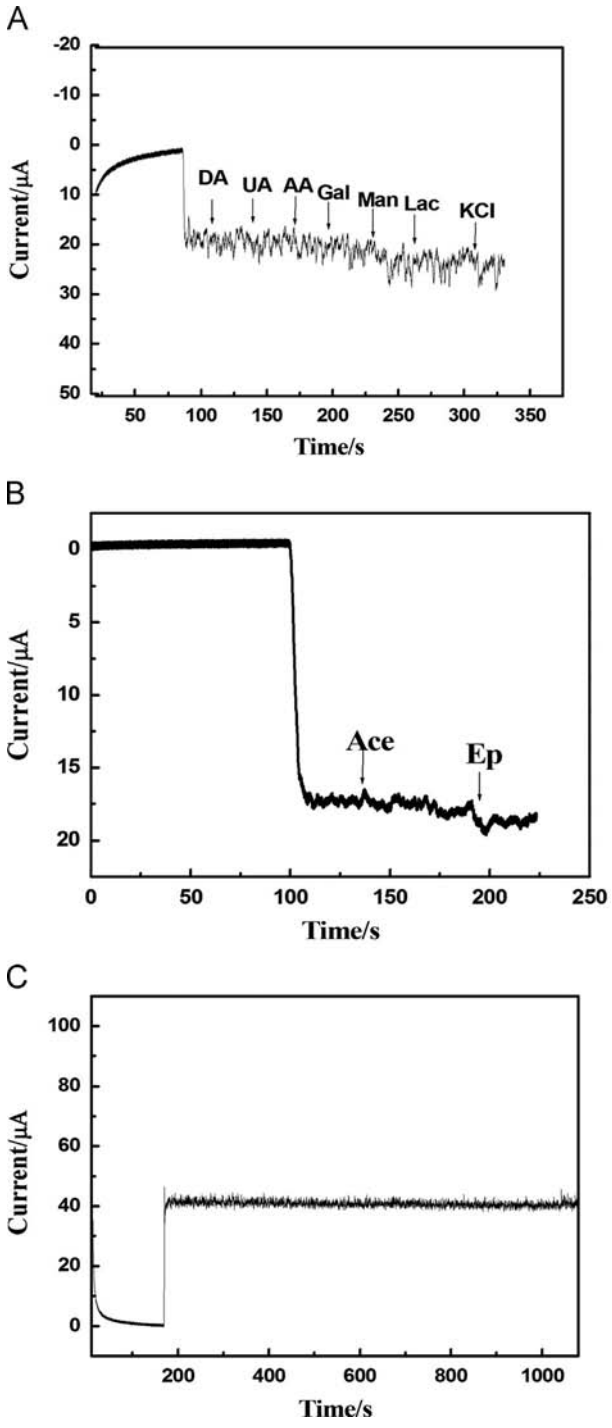

Fig. 8. Interference test of CuO/rGO/CNF/GCE in 0.1 M NaOH at +0.6 V with 0.1 mM glucose in the presence of 5 μM UA, 5 μM AA, 5 μM DA, 5 μM Gal, 5 μM Man, 5 μM Lac and 0.1 mM KCl in 0.1 M NaOH (A); interference test of CuO/rGO/CNF/GCE in 0.1 M NaOH at +0.6 V with 0.1 mM glucose in the presence of 10 μM Ace, 10 μM Ep (B) and stability tests of the CuO/rGO/CNF/GCE (C).

3.5. Reproducibility, stability and anti-interference property of the CuO/rGO/CNF/GCE

The reproducibility and storage stability of the electrode are essential for the continuous monitoring of glucose. The relative standard deviation of the current response of CuO/rGO/CNF/GCE to 0.1 mM glucose at 0.6 V was 2.2% for 10 successive measurements. This experiment confirmed that the sensor was highly reproducible. Another attractive feature of the electrode is that the response can still retain ca. 98.1% of its original signal even after it is under 0.6 V for 1000 s in a stirred solution containing 0.35 mM glucose (Fig. 8B). The long-term stability was explored by measuring 0.1 mM glucose solution intermittently, and the electrode was stored at room temperature when it was not in use. The result shows that the catalytic current response maintains 92% of its initial value after 4 weeks, reflecting the good stability of the nonenzymatic glucose sensor.

The avoidance of endogenous interfering species is a big challenge in nonenzymatic glucose detection because a few of the structurally similar organic substances (for instance, UA, DA and AA) are also simultaneously oxidized along with glucose at the electrode surface and, hence, give interfering electrochemical signals. Fig. 8A and B presents the selectivity testing results of the CuO/rGO/CNF/GCE with successive additions of 0.1 mM glucose, 5 μM UA, 5 μM AA, 5 μM DA, 5 μM galactose (Gal), 5 μM

Table 2
Determination of glucose concentration in the human saliva sample. (n=3).

Sample	Detected (μM)	Added (μM)	Found (μM)	Recovery (%)
1	83	100	182.7	99.7
2	72.1	100	173	100.9
3	62.7	100	164	101.3

mannose (Man), 5 μM lactose (Lac), 10 μM acetaminophen (Ace), 10 μM epinephrine (Ep) and 0.1 mM KCl in 0.1 M NaOH. The results show that the foreign substances do not interfere significantly on the glucose determination, in other words, the CuO/rGO/CNF/GCE presented good selectivity toward glucose detection.

3.6. Real sample analysis of the CuO/rGO/CNF/GCE based sensor

In order to verify the feasibility of the proposed method for analysis of glucose, CuO/rGO/CNF/GCE was applied to the determination of glucose in human saliva. The quantitative determination of human saliva sample was carried out using the standard addition method and the results are shown in Table 2 which was obtained as mean from three determinations. The good recovery ratios of the samples indicate that the sensor proposed in this work can be successfully applied in detecting the concentration of glucose in human saliva.

4. Conclusions

In summary, we have successfully fabricated nanoneedle CuO modified rGO/CNF film based novel non-enzymatic glucose sensor. The CuO/rGO/CNF/GCE possesses a rapid response, a low detection limit with satisfactory stability, and repeatability, and it can be used for detection of glucose content in saliva samples. Thus, the sensor carves out a noninvasive route of monitoring glucose for healthy and diabetic patients.

Acknowledgments

This work was supported by the National Natural Science Foundation of China (20890022 and 21175029) and the Shanghai Leading Academic Discipline Project (B109).

Reference

[1] J. Wang, Chem. Rev. 108 (2008) 814–825.
[2] C. Song, P.E. Pehrsson, W. Zhao, J. Mater. Res. 21 (2011) 2817–2823.
[3] P.W. Barone, R.S. Parker, M.S. Strano, Anal. Chem. 77 (2005) 7556–7562.
[4] X.W. Shen, C.Z. Huang, Y.F. Li, Talanta 72 (2007) 1432–1437.
[5] Z. Cheng, E. Wang, X. Yang, Biosens. Bioelectron. 16 (2001) 179–185.
[6] M. Morikawa, N. Kimizuka, M. Yoshihara, T. Endo, Chem. Eur. J. 8 (2002) 5580–5584.
[7] L. Meng, J. Jin, G.X. Yang, T.H. Lu, H. Zhang, C.X. Cai, Anal. Chem. 81 (2009) 7271–7280.
[8] J.P. Wang, D.F. Thomas, A.C. Chen, Anal. Chem. 80 (2008) 997–1004.
[9] W. Wang, L.L. Zhang, S.F. Tong, X. Li, W.B. Song, Biosens. Bioelectron. 25 (2009) 708–714.
[10] A. Chowdhuri, V. Gupta, K. Sreenivas, R. Kumar, S. Mozumdar, P.K. Patanjali, Appl. Phys. Lett. 84 (2004) 1180–1182.
[11] D.R. Kauffman, P.R. Ohodnicki, B.W. Kail, C. Matranga, J. Phys. Chem. Lett. 2 (2011) 2038–2043.
[12] E. Reitz, W.Z. Jia, M. Gentile, Y. Wang, Y. Lei, Electroanalysis 20 (2008) 2482–2486.
[13] G. Wang, Y. Wei, W. Zhang, X. Zhang, B. Fang, L. Wang, Microchim. Acta 168 (2010) 87–92.
[14] D. Ye, L. Luo, Y. Ding, B. Liu, X. Liu, Analyst 137 (2012) 2840–2845.
[15] D. Ye, L. Luo, Y. Ding, Q. Chen, X. Liu, Analyst 136 (2011) 4563–4569.
[16] C.Z. Yuan, B. Gao, L.F. Shen, S.D. Yang, L. Hao, X.J. Lu, F. Zhang, L.J. Zhang, X. G. Zhang, Nanoscale 3 (2011) 529–545.
[17] W.S. Hummers, R.E. Offeman, J. Am. Chem. Soc. 80 (1958) 1339–1339.
[18] S. Stankovich, D.A. Dikin, R.D. Piner, K.A. Kohlhaas, A. Kleinhammes, Y.Y. Jia, Y. Wu, S.T. Nguyen, R.S. Ruoff, Carbon 45 (2007) 1558–1565.
[19] W.-Z. Le, Y.-Q. Liu, Sens. Actuators B: Chem. 141 (2009) 147–153.
[20] D.Q. Gao, G.J. Yang, J.Y. Li, J. Zhang, J.L. Zhang, D.S. Xue, J. Phys. Chem. C 114 (2010) 18347–18351.
[21] M. Basu, A.K. Sinha, M. Pradhan, S. Sarkar, Y. Negishi, T. Pal, J. Phys. Chem. C 115 (2011) 20953–20963.
[22] I.G. Casella, M. Gatta, M.R. Guascito, T.R.I. Cataldi, Anal. Chim. Acta 357 (1997) 63–71.
[23] J. Andrzej Lasia, Electroanal. Chem. 397 (1995) 27–33.
[24] X.M. Chen, Z.J. Lin, D.J. Chen, T.T. Jia, Z.M. Cai, X.R. Wang, X. Chen, G.N. Chen, M. Oyama, Biosens. Bioelectron. 25 (2010) 1803–1808.
[25] D.B. Luo, L.Z. Wu, J.F. Zhi, ACSnano 8 (2009) 2121–2128.
[26] C.S. Shan, H.F. Yang, J.F. Song, D.X. Han, A. Ivaska, L. Niu, Anal. Chem. 81 (2009) 2378–2382.
[27] X. Kang, J. Wang, H. Wu, I.A. Aksay, J. Liu, Y. Lin, Biosens. Bioelectron. 25 (2009) 901–905.
[28] J. Luo, S. Jiang, H. Zhang, J. Jiang, X. Liu, Anal. Chim. Acta 709 (2012) 47–53.
[29] L.M. Lu, H.B. Li, F. Qu, X.B. Zhang, G.L. Shen, R.Q. Yu, Biosens. Bioelectron. 26 (2011) 3500–3504.
[30] J.C. Claussen, A. Kumar, D.B. Jaroch, M.H. Khawaja, A.B. Hibbard, D. M. Porterfield, T.S. Fisher, Adv. Funct. Mater. 22 (2012) 3399–3405.
[31] Y. Liu, H. Teng, H. Hou, T. You, Biosens. Bioelectron. 24 (2009) 3329–3334.
[32] J.H. Yuan, K. Wang, X.H. Xia, Adv. Funct. Mater. 5 (2005) 803–809.
[33] C. Shan, H. Yang, D. Han, Q. Zhang, A. Ivaska, L. Niu, Biosens. Bioelectron. 25 (2010) 1070–1074.
[34] Y. Wang, L. Liu, M. Li, S. Xu, F. Gao, Biosens. Bioelectron. 30 (2011) 107–111.
[35] X. Wang, C.G. Hu, H. Liu, G.J. Du, X.S. He, Y. Xi, Sens. Actuators B 144 (2010) 220–225.
[36] T.G. Satheesh Babu, T. Ramachandran, Electrochim. Acta 55 (2010) 1612–1618.
[37] A. Salimi, M. Roushani, Electrochem. Commun. 7 (2005) 879–887.